VETOR

Structure and photoluminescence of magnesium germanate containing tetravalent manganese as activating cation☆

Estrutura e fotoluminescência do germanato de magnésio contendo manganês tetravalente como cátion ativador

Larissa Nolding Nicolau[1,†], Ada López[1], Lilian Pantoja Sosman[1], Sandra da Silva Pedro[1]

[1]*Universidade do Estado do Rio de Janeiro, Instituto de Física Armando Dias Tavares, Rio de Janeiro, Brasil*
[†]**Autor correspondente:** larissanolding@yahoo.com.br

Abstract

The aim of the current study is to present the acetate method synthesis of magnesium germanate (Mg_2GeO_4) compound containing Mn^{4+} as activating cation for optical transitions. The crystalline structure of this compound was investigated through X-ray diffraction measurements in association with the Rietveld method, which confirmed the formation of the intended compound. Photoluminescence spectroscopy measurements have shown emission in the red region. The emission spectrum under 287 nm excitation presented an intense peak at 660 nm, followed by several structures. Optical transitions were identified and confirmed Mn^{4+} occupation in octahedral symmetry. Crystal field parameter Dq and Racah parameters B and C, were calculated based on optical spectra. Emission lifetime was 2.8 ms, and it was compatible to the spin-forbidden electronic transition $^2E(^2G) \rightarrow {}^4A_2(\,{}^4F)$ attributed to the emission at 660 nm. The current findings pointed out that the sample was successfully synthesized, and that its optical properties can be used in devices that operate with emission in the red range of the visible spectrum.

Keywords

Ceramics • X-ray diffraction • Photoluminescence • Mn^{4+}

Resumo

Apresentamos a síntese pelo método do acetato do composto germanato de magnésio (Mg_2GeO_4) contendo Mn^{4+} como cátion ativador de transições ópticas. A estrutura cristalina do composto foi caracterizada através de medidas de difração de raios-X em conjunto com o método de Rietveld, que confirmaram a formação do composto pretendido. Medidas de espectroscopia de fotoluminescência mostram uma emissão na região do vermelho. Sob excitação de 287 nm, o espectro de emissão exibe um pico intenso em 660 nm, acompanhado de diversas estruturas. As transições ópticas foram identificadas e confirmam a ocupação do Mn^{4+} em simetria octaédrica. A partir dos espectros ópticos os parâmetros de campo cristalino Dq, B e C foram calculados. O tempo de vida da emissão é da ordem de 2,8 ms, compatível com a transição eletrônica proibida por spin $^2E(^2G) \rightarrow {}^4A_2(^4F)$ atribuída à emissão em

☆ This article is an extended version of the work presented at the Joint XXVII ENMC National Meeting of Computational Modeling, XV ECTM Meeting of Materials Science and Technology, held at Ilhéus, Bahia, from October 1st to 4th, 2024.

660 nm. Os resultados indicam que a amostra foi sintetizada com sucesso e as suas propriedades ópticas podem ser aproveitadas em dispositivos que operam com emissão na faixa do vermelho no espectro visível.

Palavras-chave

Cerâmicas • Difração de raios-X • Fotoluminescência • Mn^{4+}

1 Introduction

Magnesium germanate (Mg_2GeO_4) ceramics is a promising compound for developing new materials to be used in thermoelectric power generation systems [1], plasma panels [2], materials with dielectric properties for microwave-based devices [3, 4] and optical information security [5], among other applications. Germanates are also attractive materials due to the abundance and relatively low cost of preparation reagents, as well as to their low toxicity, reasonable conductivity and high stability [1, 6].

The Mn^{4+} cation has $3d^3$ electronic configuration, besides preferably occupying positions with octahedral symmetry when it is inserted into a host lattice [7, 8, 9, 10]. Mn^{4+} insertion into a given host splits the energy levels of free-ion's d electronic orbitals, as well as leads to considerable occupancy site distortion, a fact that generates emission and absorption bands in the UV-VIS-NIR regions. Ceramics containing Mn^{4+} transition metal cations as emitting center are examples of materials that have been extensively investigated, since they show luminescence in the red-infrared region (650-750 nm) when they absorb radiation in the ultraviolet-blue region (250-500 nm). The relevance of these materials can be seen in the following examples: they can be used as source of lighting for plants' cultivation and growth purposes, since their red emission stimulates photosynthesis [9, 11]; they can also be used to develop WLEDs (white light emitting diodes) and pc-LEDs (phosphor-converted light emitting diodes) to be used in displays, vehicles, telecommunications, medicine and general lighting [7, 8, 12, 13]. Their luminescence can be tuned to meet specific technological needs depending on the properties of the crystal lattice the ion is inserted in. In other words, it is possible to control the emission's wavelength and intensity, depending on the cation-host lattice interaction and on the covalence degree of the bond between the activating cation and ligand anions [8].

Xue et al. [13] produced Mg_2GeO_4 samples with varying Mn^{4+} concentrations and observed an intense emission at 659 nm. Mg_2GeO_4 is successfully synthesized through the solid-state method [2, 4, 6, 13].

The aim of the current study was to propose and present the results of Mg_2GeO_4 ceramics production based on using 0.1 at. mol% Mn^{4+} as substitutional ion, in compliance with the acetate method. To the best of our knowledge, this was the first time this compound was synthesized through this preparation method. Crystallographic features were analyzed through X-ray diffraction and Rietveld method. The sample's optical properties were investigated through photoluminescence spectroscopy. Emission and excitation spectra were used to identify electronic transitions to calculate crystal field parameters. Furthermore, lifetime measurements enabled identifying the prevalent excited state-relaxation process. Findings in the current study pointed out that the acetate method is efficient in preparing the investigated compound, and sample's emission has shown that it can have optical applications in the red range of the visible spectrum.

2 Materials and Methods

2.1 Synthesis

The ceramics production process started with ultrapure reagents' selection to prepare the Mg_2GeO_4 compound containing 0.1 at. mol% of MnO_2.MgO (magnesium oxide, Riedel de Häen, ≥ 99%), GeO_2 (germanium dioxide, Sigma-Aldrich, 99.99%) and MnO_2 (manganese oxide, Sigma-Aldrich, 99.99%) were used as reagents. MgO is a highly hygroscopic compound [15], and this behavior increases the likelihood of forming unwanted phases in the sample. When MgO mass is measured, a large amount of water absorbed by the oxide is also measured, and it generates MgO deficit in the reaction. Consequently, the reaction between reactants may not fully happen, and it leads to the emergence of undesirable phases in the sample. Therefore, it was used MgO mass in an amount of 50% over the reaction's stoichiometry to guarantee the formation of the maximum Mg_2GeO_4 phase.

Reagents were weighed on precision scale. Then, sample homogenization began; this process lied on preparing a solution in glass beaker filled with 50% deionized water and 50% glacial acetic acid (CH_3CO_2H). Reagents were added to the solution in order to form a mix that was subsequently placed on a hot plate equipped with magnetic stirrer. The liquid part of the solution evaporated after 1-hour mixing on the heating plate and the remaining solid part was placed in oven to thoroughly dry the material. The material was removed from the oven 24 hours later and

homogenized with a pestle in agate mortar for a few minutes to decompress and to produce a fine powder. The powder was deposited in alumina crucible and subjected to the first thermal treatment in muffle furnace at 700 °C, for 6 hours. The compound was decompressed again in agate mortar, after it was removed from the oven. The resulting material was split into three equal fractions that were pressed at 294 MPa, to form tablets measuring 13 mm, in diameter and 1 mm, in thickness. The pellets were placed again in alumina crucibles and subjected to a new heat treatment in muffle furnace at 1,250 °C, for 6 hours, in order to sinter the compound. At the end of the heat treatment, the oven was turned off and the sample remained inside it until it reached room temperature due to the oven's inertia.

2.2 XRD Analysis and Photoluminescence Spectroscopy

One of the pellets was pulverized for powder X-ray diffraction (XRD) measurements, which were taken at room temperature in Bruker D2 PHASER diffractometer equipped with copper anode - it operated at voltage of 30 kV, current of 10 mA and Cu-Kα radiation wavelength ($\lambda = 1.54180$ Å). The diffractogram was generated a step of 0.01° in a sweep of 2θ angles in the range $10° < 2\theta < 80°$. Rietveld refinement was performed in FullProf free access software [16], based on XRD data, through which the lattice parameters, the quantitative proportion of the phases present in the synthesized sample, and the atomic positions were determined.

Photoluminescence spectroscopy measurements (emission, excitation and lifetime) were taken in PTI 300 Quanta Master UV-VIS spectrofluorometer equipped with 75 W pulsed xenon lamp, which was used as excitation source. Measurements were taken at step of 1 nm, slits of 3 nm and signal modulated at 200 Hz. All spectra were detected on PTI 914 photomultiplier (operation range 185-900 nm, peak at 400 nm). Equipment control and data storage were carried out in Felix GX software. Newport filters were used to block excitation wavelengths and scattered light within the experimental apparatus. All optical spectra were corrected by taking into consideration the spectral response of the experimental apparatus.

3 Results and Discussion

Figure 1 shows the X-ray diffractogram (XRD) of the synthesized sample. It also shows the respective Rietveld refinement obtained from XRD data.

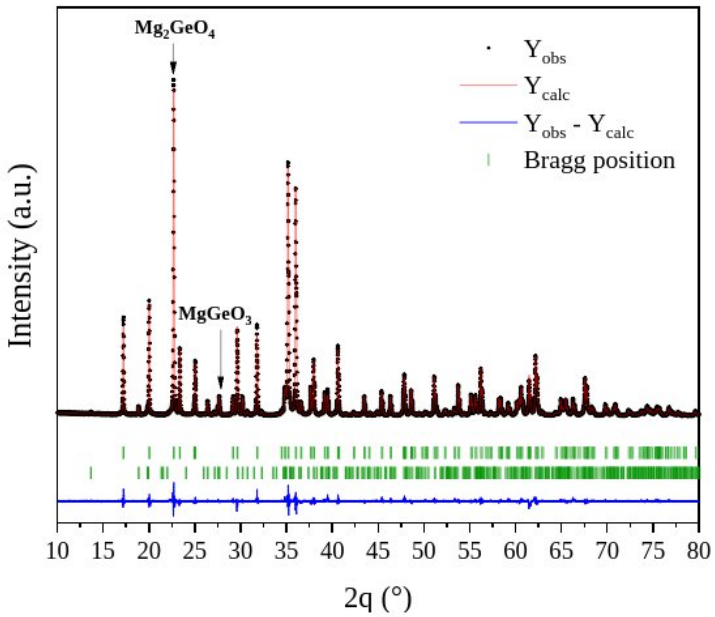

Figure 1: X-ray diffractogram of the sample and the respective Rietveld refinement.

Black dots represent the experimental data, the red line is the calculated fit, the blue line is the difference between the observed and calculated data, and the green dashes represent the Bragg positions of the peaks in the formed phases (at the top, the peaks of the Mg_2GeO_4 phase; at the base, the $MgGeO_3$ peaks). The arrows indicate the highest intensity peak of the respective formed phases.

XRD experimental peak profile patterns were compared to the crystallographic base pattern profiles of the Mg_2GeO_4 compound and of likely compounds formed from the precursors. Based on results obtained through Rietveld refinement, the ceramic sample presented the desired main phase (Mg_2GeO_4), at the proportion of approximately 92% of the total mass recorded for the sample, as well as a secondary phase ($MgGeO_3$) at the proportion of 8% of it. The Inorganic Crystal Structure Database (ICSD) files #41415 for the Mg_2GeO_4 compound and ICSD #201665 for $MgGeO_3$ identified the corresponding phases.

Table 1: Crystallographic parameters of the identified phases and Rietveld refinement quality.

Lattice Parameters						
Phases	Proportion (%)	a (Å)	b (Å)	c (Å)	V $(Å^3)$	$\alpha = \beta = \gamma$ (°)
Mg_2GeO_4	91.73	10.300(4)	6.028(4)	4.909(6)	304.859(6)	90
$MgGeO_3$	8.27	18.803(9)	8.949(0)	5.341(4)	898.821(4)	90
Refinement Quality						
R_{wp} (%)		R_p (%)		R_{exp} (%)	χ^2	GoF
9.64		8.50		5.87	2.69	1.6

Crystallographic parameters deriving from Rietveld refinement are shown in Table 1. The Mg_2GeO_4 phase crystallized into orthorhombic symmetry, space group *Pnma*, with lattice parameters a = 10.300 Å, b = 6.028 Å and c = 4.909 Å, unit cell volume V = 304.859 $Å^3$. The angles α, β, and γ in Table 1 are the angles between the unit cell axes. The additional $MgGeO_3$ phase also presented orthorhombic symmetry, space group *Pbca*, with lattice parameters a = 18.803 Å, b = 8.949 Å and c = 5.341 Å. The refinement quality parameters (Table 1) have evidenced that the refinement process was successful. The Goodness of Fit parameter ($GoF = R_{wp}/R_{exp}$) attesting to refinement quality reached 1.6, which indicated that the refinement was satisfactory for a two-phase crystalline system [14]. The small amount of secondary phase $MgGeO_3$ (8%) makes it unlikely that Mn^{4+} will occupy this structure's positions. Based on the observed values of lattice parameters, Mn^{4+} cation insertion into the structure did not significantly change the crystallographic structure of the main phase. Table 2 describes ions' oxidation states and atomic positions (X, Y, Z) in the Mg_2GeO_4 phase. The Wyckoff symbols (letters a, c, d) indicate the coordinates allowed by symmetry elements used to describe the atoms' positions in a crystalline structure, and the numbers following the letters indicate the multiplicity of these positions.

Table 2 – Oxidation state, Wyckoff symbols and atomic positions of the Mg_2GeO_4 phase.

Atom	Oxidation	Wyckoff	X	Y	Z
Mg1	+2	4a	0.09484	0.25000	0.43709
Mg2	+2	4c	0.27741	0.25000	0.98981
Ge1	+4	4c	0.09484	0.25000	0.43709
O1	-2	4c	0.08901	0.25000	0.79253
O2	-2	4c	0.44207	0.25000	0.23313
O3	-2	8d	0.16189	0.02205	0.26934

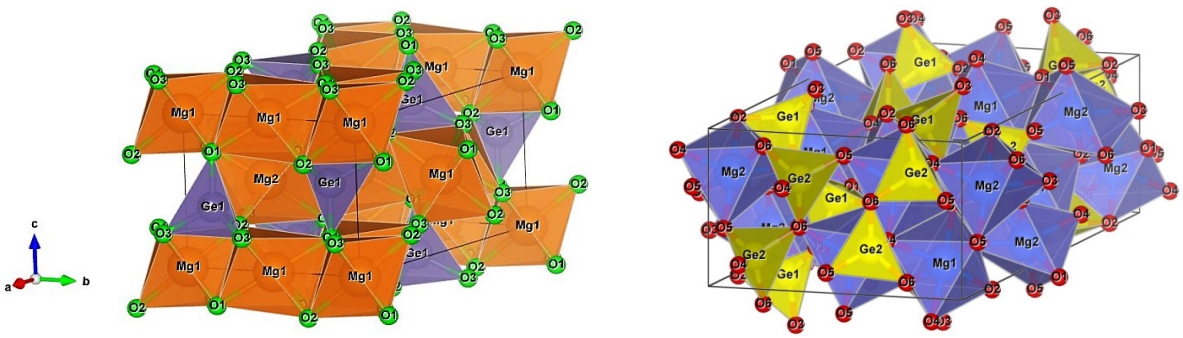

(a) Mg_2GeO_4 (b) $MgGeO_3$

Figure 2: Representations of unit cells of the (a) Mg_2GeO_4 and (b) $MgGeO_3$ phases simulated in Visualization for Electronic and Structural Analysis (VESTA) software.

Figure 2 shows the representation of Mg_2GeO_4(a) and $MgGeO_3$(b) phase crystal structures, which were generated in VESTA free software [17]. (a) In the main phase Mg_2GeO_4, Ge^{4+} ions occupy tetrahedral symmetry sites (violet), whereas Mg^{2+} occupies octahedral symmetry sites (orange). The same behavior is observed in the secondary phase (b) $MgGeO_3$, wherein Ge^{4+} ions occupy tetrahedral symmetry sites (yellow), whereas Mg^{2+} occupies octahedral symmetry sites (blue).

Figure 3(a) shows the photoluminescence emission and excitation spectra. The emission spectrum (in red) was obtained at excitation wavelength of 287 nm. It shows two narrow peaks followed by superimposed structures on the peaks. Compound's emission took place in the red range; the most intense emission peak was observed at 660 nm (15,151 cm^{-1}) and a structure was observed at 653 nm (15,314 cm^{-1}). A second lower-intensity peak was observed at 633 nm (15,798 cm^{-1}), it was followed by structures positioned at 626 nm (15,974 cm^{-1}) and 643 nm (15,552 cm^{-1}). Intense and narrow peak at 660 nm was identified as R line (or zero-phonon line (ZPL)) of the spin-forbidden transition $^2E(^2G) \rightarrow {}^4A_2(^4F)$ of Mn^{4+} in octahedral coordination site. The presence of peak at 653 nm and the different structures observed close to 660 nm emission can be attributed to Mn^{4+} occupation in different sites, and it suggests that the octahedral sites in the Mg_2GeO_4 structure were not equivalent [5, 18, 19]. The Mg^{2+} atoms in Table 2 occupy two different octahedral positions with different distortion degrees, as indicated by Wyckoff sites 4a (Mg1) and 4c (Mg2). According to Jiang et al. [19], Mg1 cations occupy octahedra presenting edge shared with other neighboring octahedra, which are also occupied by Mg1 cations and form a one-dimensional chain. The octahedra occupied by Mg2 cations work as “bridges” connecting the chains of octahedra occupied by Mg1 cations.

The excitation spectrum (seen in black in Figure 3(a)) was obtained by emission positioned at 660 nm. It showed two broad bands in the ultraviolet-blue region with maxima at 286 nm (34,965 cm^{-1}) and 421 nm (23,753 cm^{-1}). The excitation spectrum was multiplied by 3 as comparison criterion. The highest energy band of the excitation spectrum with maximum of 286 nm was deconvolved based on using Gaussian fit, as shown in Figure 3(b) [9]. Band deconvolution has shown that it comprises two bands centered at 279 nm (35,824 cm^{-1}) and 307 nm (32,573 cm^{-1}). The band observed at 307 nm was attributed to the spin allowed transition $^4A_2(^4F) \rightarrow {}^4T_1(^4F)$, whereas the band positioned at 421 nm was related to the $^4A_2(^4F) \rightarrow {}^4T_2(^4F)$ transition. The band in the highest energy region (279 nm) was associated with the $O^{2-} \rightarrow Mn^{4+}$ ligand-metal charge transfer process [7, 8, 9]. Both the emission and excitation bands corroborated the optical spectra observed by Xue *et al.* [13] in the Mg_2GeO_4:Mn^{4+} compound. Both emission and excitation spectra pointed out that Mn^{4+} was successfully inserted into the octahedral sites of the Mg_2GeO_4 host lattice.

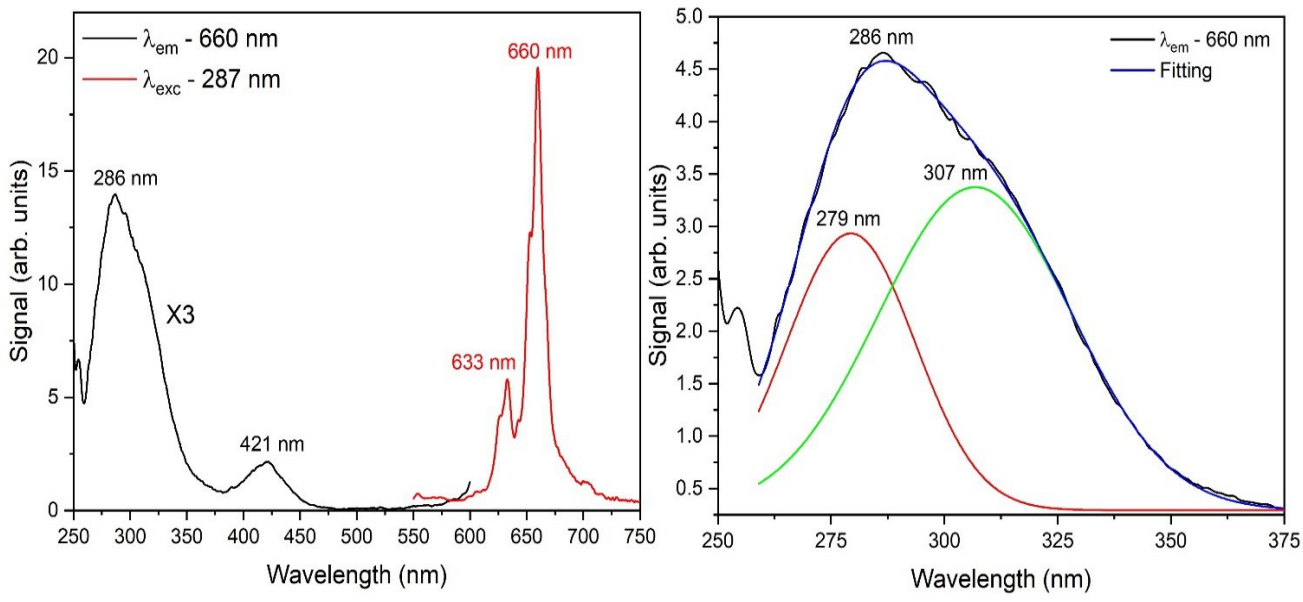

Figure 3: (a) Excitation (in black) and emission (in red) spectra of the sample. The excitation spectrum was multiplied by 3 for comparison purposes. (b) Detail of the band with a maximum excitation spectrum at 286 nm. The deconvolution of this band shows good result for the hypothesis, according to which, it is composed of two bands, with maxima intensities at 279 nm and 307 nm.

Optical spectra interpretation requires understanding the crystalline structure occupied by the activating cation, in this case, Mn^{4+}. A cation can be substitutionally inserted into a host lattice when it meets criteria, such as affinity with the symmetry of the occupation site, proximity between ionic radii values, and similar valences. Several authors have mentioned that Mn^{4+} preferably occupies sites with octahedral symmetry [7, 8, 9, 10]. With respect to ionic radii, occupancy is viable if the rate difference between the ionic radii of the lattice cations and the substitutional cation is lower than 30% [9]. If one takes into consideration the ionic radii of Mg^{2+} (0.72 Å) and Mn^{4+} (0.53 Å) cations, both for octahedral symmetry (NC = 6, wherein NC is the coordination number), the rate difference between the substituted and substitute cation is close to 26%, and it enables replacing Mg^{2+} with Mn^{4+} in octahedral coordination sites, as well as forming light emitting [MnO_6] centers [13].

There was a difference between valences of cations involved in the cation substitution process, which led to cation distortion and to defects in the host lattice. According to Srivastava *et al.* [8], the emergence of defects or cationic disorder can be beneficial to Mn^{4+} emission in octahedral symmetry, since such disorders increase the R line intensity due to decreased symmetry around the Mn^{4+} cation. The analysis of the aforementioned criteria confirmed the attribution of electronic transitions observed in the optical spectra, according to which, Mn^{4+} occupied octahedral sites and replaced Mg^{2+}.

The crystal field parameters Dq and Racah parameters B and C were determined using the values of the transition energies observed in the excitation spectrum in the equations below extracted from the Tanabe-Sugano matrices for d^3 systems in octahedral environment [8, 9, 11, 10]:

$$E\left({}^4T_2\right) = 10\,Dq \tag{1}$$

$$B = \frac{\left(\frac{\Delta E}{Dq}\right)^2 - 10\left(\frac{\Delta E}{Dq}\right)}{15\left[\left(\frac{\Delta E}{Dq}\right) - 8\right]}\,Dq \tag{2}$$

$$C \cong 0.328\Delta E - 2{,}59B + \frac{0{,}59B^2}{Dq} \tag{3}$$

Where $\Delta E = E\left({}^4T_1\right) - E\left({}^4T_2\right)$ is the energy difference between the $^4T_1(^4F)$ and $^4T_2(^4F)$ states. The crystal field parameter value obtained was Dq = 2,375 cm^{-1} and the Racah parameters were calculated to be B = 855 cm^{-1} and C = 2,937 cm^{-1}. The Dq/B ≈ 2.78 ratio pointed out strong crystal field, since the threshold for Dq/B values accounting for differentiating strong from weak crystal fields is approximately 2.2 [9]. The character of the Mn-O bond can be estimated based on the value observed for the nepheulaxetic parameter (Eq. (4)) [8],

$$\beta_1 = \sqrt{\left(\frac{B}{B_0}\right)^2 + \left(\frac{C}{C_0}\right)^2} \tag{4}$$

wherein B_0 = 1,160 cm^{-1} and C_0 = 4,303 cm^{-1} are the Racah parameters for the free Mn^{4+} ion [8]. The lower the β_1 value, the greater the Mn-O bond covalency. β_1 value equals to 1.004 was calculated for Mg_2GeO_4:Mn^{4+}, and it suggested strongly covalent bond in comparison to other Mn^{4+} based systems [8].

Figure 4(a) shows the emission decay profile of the sample monitored at emission peak positioned at 660 nm, with excitation wavelength of 287 nm. Experimental data were fitted by using a simple exponential decay function, according to which, decay was mostly caused by radiative processes. Photoluminescence lifetime was estimated at 2.8 ms based on the experimental data fit; this value lies on the same order of magnitude observed for other oxide systems presenting Mn^{4+} as an activating ion in octahedral coordination [7, 8]. The R-squared value close to 1 indicates an excellent adjustment of decay data. Lifetime indicates the nature of the photoluminescent emission. Short lifetime emissions (in the order of microseconds) are associated with spin-allowed transitions. They are more likely to happen, whereas long-lifetime emissions (milliseconds or more) suggest forbidden transitions with lower transition likelihood. The observed long- lifetime emission pointed out that the transition related to the emission observed at 660 nm was the spin forbidden transition $^2E(^2G) \rightarrow {}^4A_2(^4F)$, and it confirmed the assignment of this initially presented emission.

Figure 4(b) shows the sample chromaticity coordinate diagram, whose emission is in the red range with coordinates x = 0.662 and y = 0.334. Color purity was estimated at 83.91% based on using the Color Purity Calculator

for luminescence spectrum applet (1931), available at https://sciapps.sci-sim.com/color_purity.html [20], and it evidenced high purity red emission. Emission band-color purity is an essential factor used to assess the quality of emitting materials. High color-purity materials are potential components for full-color spectrum-generating devices

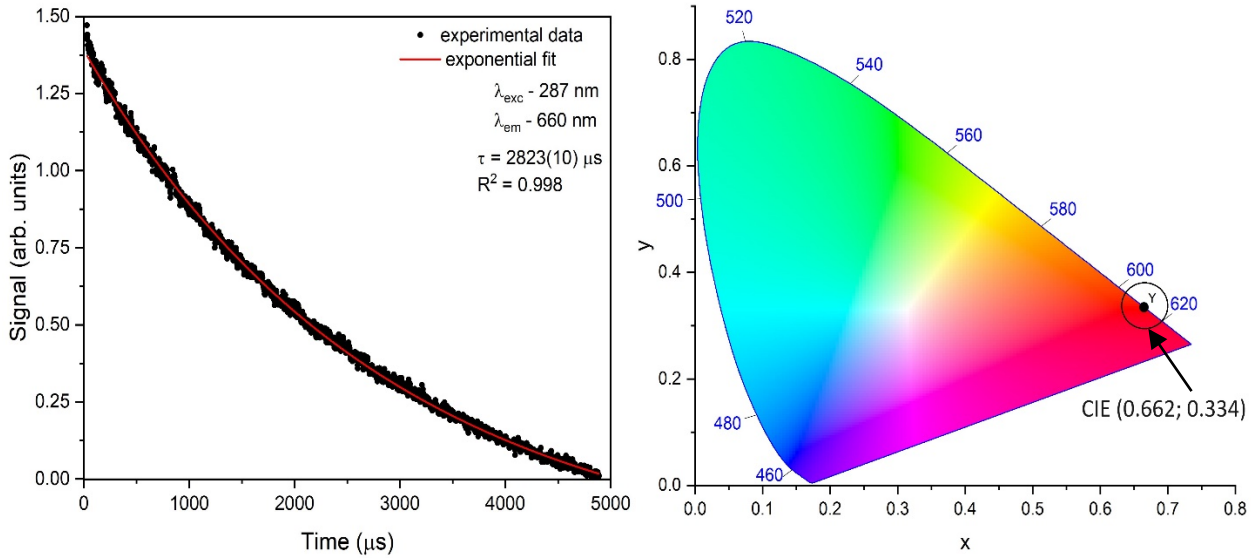

Figure 4: (a) Emission decay curve monitored at 660 nm, under 287 nm excitation. The experimental points are highlighted in black, and the red curve shows the fit of the experimental data based on a single exponential-type function. (b) CIE 1931 chromaticity coordinate diagram corresponding to the sample emission color.

and for other emitting systems with complementary color emission bands. Therefore, this material type has strong potential to be used as an emission source in the red region of the electromagnetic spectrum.

4 Conclusions

The $Mg_2GeO_4:Mn^{4+}$ ceramic was synthesized based on the acetate method. It remains unknown whether this method had been previously used to produce this material. Quantitative phase analysis based on using the Rietveld method to refine X-ray diffraction data has evidenced that the sample comprised 92% of the Mg_2GeO_4 phase and 8% of the $MgGeO_3$ secondary phase. The sample presented emission in the red region showing a narrow band positioned at 660 nm, which was followed by several structures under excitation wavelength of 287 nm. This band was identified as the spin-forbidden electronic transition $^2E(^2G) \rightarrow {}^4A_2(^4F)$. The relatively long emission lifetime (2.8 ms) confirmed the transition attributed to the emission, and the exponential character of the decay pointed out that the relaxation of the excited state mostly happened due to radiative processes. The excitation spectrum related to the 660 nm emission presented two bands in the ultraviolet-blue region - the highest energy band comprised two strongly overlapping bands: one of them was identified as charge transfer band (279 nm), whereas the other one was attributed to the spin- allowed transition $^4A_2(^4F) \rightarrow {}^4T_1(^4F)$, at 307 nm. A second band at lower energy (421 nm) was attributed to the spin-allowed electronic transition $^4A_2(^4F) \rightarrow {}^4T_2(^4F)$. Electronic transitions identified in the optical spectra were associated with the insertion of Mn^{4+}, which occupied two non-equivalent octahedral sites. The current findings pointed out that the sample was successfully synthesized, and that its optical properties can be used in devices that operate by emission in the red range of the visible spectrum.

Acknowledgements

This study was financed in part by the Coordenação de Aperfeiçoamento de Pessoal de Nível Superior – Brasil (CAPES) – Finance Code 001. The authors would also like to thank Fundação Carlos Chagas de Amparo à Pesquisa do Estado do Rio de Janeiro (FAPERJ) for the financial assistance, and Laboratório de Instrumentação e Técnicas Analíticas (LIETA/UERJ) for carrying out the X-ray diffraction measurements. S. S. Pedro and L. P. Sosman are grateful to CNPq (Conselho Nacional de Desenvolvimento Científico e Tecnológico) for research productivity grants. S. S. Pedro thanks FAPERJ for Jovem Cientista do Nosso Estado (JCNE) grant.

References

[1] K. Mahmood, J. Jacob, A. Rehman, A. Ali, U. Rehaman, N. Amin, S. Ikram, A. Ashfaq, and S. Hussain, "Modulation of thermoelectric properties of Mg_2GeO_4 thin films by controlling the growth process," *Ceramics International*, vol. 45, no. 15, pp. 18701–18703, 2019. Available at: https://doi.org/10.1016/j.ceramint.2019.06.095

[2] H. M. Yang, J. X. Shi, H. B. Liang, and M. L. Gong, "A novel red phosphor Mg_2GeO_4 doped with Eu^{3+} for PDP applications," *Materials Science and Engineering: B*, vol. 127, no. 2–3, pp. 276–279, 2006. Available at: https://doi.org/10.1016/j.mseb.2005.10.014

[3] C. X. Chen, S. P. Wu, and Y. X. Fan, "Synthesis and microwave dielectric properties of B_2O^{3-} doped Mg_2GeO_4 ceramics," *Journal of Alloys and Compounds*, vol. 578, pp. 153–156, 2013. Available at: https://doi.org/10.1016/j.jallcom.2013.05.038

[4] S. Deng, X. Qu., X. Wang, Y. Xiao, G. He, K. Liu, Q. Li, Z. Dai, X. Chen, and H. Zhou, "Solid-phase reaction mechanism and microwave dielectric properties of Mg_2GeO_4-$MgAl_2O_4$ composite ceramics," *Ceramics International*, vol. 48, no. 21, pp. 31890–31895, 2022. Available at: https://doi.org/10.1016/j.ceramint.2022.07.122

[5] J. Yang, Y. Zhou, H. Ming, E. Song, and Q. Zhang, "Site-selective occupancy of Mn^{2+} enabling adjustablered/near-infrared multimode luminescence in olivine for dynamic anticounterfeiting and encryption," *Applied Electronic Materials*, vol. 4, no. 2, pp. 831–841, 2022. Available at: https://doi.org/10.1021/acsaelm.1c01182

[6] H. M. Yang, Z. Wang, M. L. Gong, and H. Liang, "Luminescence properties of a novel red emitting phosphor, Mg_2GeO_4:Sm^{3+}," *Journal of Alloys and Compounds*, vol. 488, no. 1, pp. 331–333, 2009. Available at: https://doi.org/10.1016/j.jallcom.2009.08.123

[7] X. Wang, P. Li, M. G. Brik, X. Li, L. Li, and M. Peng, "Thermal quenching of Mn^{4+} luminescence in $SrAl_{12}O_{19}$:Mn^{4+}," *Journal of Luminescence*, vol. 206, pp. 84–90, 2019. Available at: https://doi.org/10.1016/j.jlumin.2018.10.044

[8] A. M. Srivastava, M. G. Brik, C.G. Ma, W. W. Beers, W. E. Cohen, and M. Piasecki, "Effect of covalence and degree of cation order on the luminous efficacy of Mn^{4+} luminescence in the double perovskites, Ba_2BTO_6 (B = Y, Lu, Sc)," *The Journal of Physical Chemistry Letters*, vol. 15, no. 15, pp. 4175–4184, 2024. Available at: https://doi.org/10.1021/acs.jpclett.4c00205

[9] W. Zou, R. Zhu, X. Zhang, Y. Li, J. Zuo, P. He, J. Zhang, W. Wang, J. Peng, and X. Ye, "Enhancing the luminescence of Mn^{4+}-doped double perovskite oxide Ca_2LuNbO_6 phosphor by utilizing A-site cationic fluoride as a flux," *Ceramics International*, vol. 50, no. 13, pp. 22627–22636, 2024. Available at: https://doi.org/10.1016/j.ceramint.2024.03.364

[10] S. Adachi, "Photoluminescence properties of Mn^{4+}-activated oxide phosphors for use in white-LED applications: A review," *Journal of Luminescence*, vol. 202, pp. 263–281, 2018. Available at: https://doi.org/10.1016/j.jlumin.2018.05.053

[11] H. Liu; J. Liu, B. Sun, Z. Zhang, C. Jiao, D. Sun, L. Zhang, and Y. Zhang, "Ca_2LaTaO_6:Bi^{3+}/Mn^{4+} phosphors with high brightness far-red emitting and luminescence enhancement for plant growth LED lights and temperature sensor," *Inorganic Chemistry*, vol. 63, pp. 5365–5377, 2024. Available at: https://doi.org/10.1021/acs.inorgchem.3c03939

[12] M. Peng, X. Yin, P. Tanner, M. G. Brik, and P. Li, "Site occupancy preference, enhancement mechanism, and thermal resistance of Mn^{4+} red luminescence in $Sr_4Al_{14}O_{25}$:Mn4+ for warm WLEDS," *Chemistry of Materials*, vol. 27, no. 8, pp. 2938–2945, 2015. Available at: https://doi.org/10.1021/acs.chemmater.5b00226

[13] F. Xue, Y. Hu, L. Chen, H. Wu, G. Ju, T. Wang, and L. Yang, "A novel rare-earth free red long-persistent phosphor: Mg_2GeO_4:Mn^{4+}," *Ceramics International*, vol. 43, no. 17, pp. 15141-15145, 2017. Available at: https://doi.org/10.1016/j.ceramint.2017.08.044

[14] B. H. Toby, "R factors in Rietveld analysis: How good is good enough?," *Powder diffraction*, vol. 21, no. 1, pp. 67–70, 2006. Available at: https://doi.org/10.1154/1.2179804

[15] N. D. C. Santana, A. López, L. P. Sosman, and S. S. Pedro, "Photoluminescence of tetrahedrally coordinated Co^{2+} in magnesium titanate," *Optical Materials*, vol. 134, pp. 113119, 2022. Available at: https://doi.org/10.1016/j.optmat.2022.113119

[16] J. Rodríguez-Carvajal, "Recent advances in magnetic structure determination by neutron powder diffraction," *Physica B: Condensed Matter*, vol. 192, no. 1–2, pp. 55–69, 1993. Available at: https://doi.org/10.1016/0921-4526(93)90108-I

[17] K. Momma and F. Izumi, "VESTA 3 for three-dimensional visualization of crystal, volumetric and morphology data", *Journal of Applied Crystallography*, vol. 44, no. 6, pp. 1272–1276, 2011. Available at: https://doi.org/10.1107/s0021889811038970

[18] H. Cai, S. Liu, Z. Song, and Q. Liu, "Tuning luminescence from NIR-I to NIR-II in Cr^{3+} -doped olivine phosphors for nondestructive analysis," *Journal of Materials Chemistry C*, vol. 9, no. 16, pp. 5469–5477, 2021. Available at: https://doi.org/10.1039/D1TC00521A

[19] B. Jiang, B. Lou, Q. Liu, J. Zhang, F. Chi, and J. Zhang, "Investigation on the valence state stability and optical properties of Mg_2GeO_4:Cr," *Optical Materials,* vol. 150, pp. 115136, 2024. Available at: https://doi.org/10.1016/j.optmat.2024.115136

[20] E. H. H. Hasabeldaim, H. C. Swart, and R. E. Kroon, "Luminescence and stability of Tb doped CaF2 nanoparticles," *Royal Society of Chemistry*, vol. 13, no. 8, pp. 5353–5366, 2023. Available at: https://doi.org/10.1039/d2ra07897j